Molecular Biology of the Cell
Vol. 18, 3131–3143, August 2007

Fast Turnover of L1 Adhesions in Neuronal Growth Cones Involving Both Surface Diffusion and Exo/Endocytosis of L1 Molecules[D] [V]

Caroline Dequidt,* Lydia Danglot,† Philipp Alberts,† Thierry Galli,† Daniel Choquet,* and Olivier Thoumine*

*Unité Mixte de Recherche Centre National de la Recherche Scientifique 5091, Institut François Magendie, Université Bordeaux 2, 33077 Bordeaux, France; and †Membrane Traffic in Epithelial and Neuronal Morphogenesis, Equipe Avenir Inserm, Institut Jacques Monod, Unité Mixte de Recherche Centre National de la Recherche Scientifique 7592, Universités Paris 6 et 7, 75251 Paris, France

Submitted December 13, 2006; Revised May 7, 2007; Accepted May 18, 2007
Monitoring Editor: Paul Forscher

We investigated the interplay between surface trafficking and binding dynamics of the immunoglobulin cell adhesion molecule L1 at neuronal growth cones. Primary neurons were transfected with L1 constructs bearing thrombin-cleavable green fluorescent protein (GFP), allowing visualization of newly exocytosed L1 or labeling of membrane L1 molecules by Quantum dots. Intracellular L1–GFP vesicles showed preferential centrifugal motion, whereas surface L1–GFP diffused randomly, revealing two pathways to address L1 to adhesive sites. We triggered L1 adhesions using microspheres coated with L1–Fc protein or anti-L1 antibodies, manipulated by optical tweezers. Microspheres coupled to the actin retrograde flow at the growth cone periphery while recruiting L1–GFP molecules, of which 50% relied on exocytosis. Fluorescence recovery after photobleaching experiments revealed a rapid recycling of L1–GFP molecules at L1–Fc (but not anti-L1) bead contacts, attributed to a high lability of L1–L1 bonds at equilibrium. L1–GFP molecules truncated in the intracellular tail as well as neuronal cell adhesion molecules (NrCAMs) missing the clathrin adaptor binding sequence showed both little internalization and reduced turnover rates, indicating a role of endocytosis in the recycling of mature L1 contacts at the base of the growth cone. Thus, unlike for other molecules such as NrCAM or N-cadherin, diffusion/trapping and exo/endocytosis events cooperate to allow the fast renewal of L1 adhesions.

INTRODUCTION

Cell adhesion molecules of the immunoglobulin superfamily (IgCAMs), including L1, play essential roles in the developing nervous system. Indeed, pathological mutations in the L1 gene are related to a variety of neurological disorders in humans, including mental retardation and hydrocephalus (De Angelis *et al*., 1999). L1 knockout mice also show severe brain abnormalities (Kamiguchi *et al*., 1998a; Itoh *et al*., 2004). IgCAMs mediate axonal elongation, fasciculation, and guidance. These functions involve both homophilic and heterophilic adhesions between IgCAM members as well as anchoring of ligand-bound receptors to the actin cytoskeleton, which allows for force transmission and enables neuronal growth cones to move forward (Suter *et al*., 1998; Brummendorf and Lemmon, 2001).

This article was published online ahead of print in *MBC in Press* (http://www.molbiolcell.org/cgi/doi/10.1091/mbc.E06–12–1101) on May 30, 2007.

[D] [V] The online version of this article contains supplemental material at *MBC Online* (http://www.molbiolcell.org).

Address correspondence to: Olivier Thoumine (olivier.thoumine@pcs.u-bordeaux2.fr).

Abbreviations used: DIV, days in vitro; DRG, dorsal root ganglion; L1–Fc, L1 extracellular domain fused to human Fc; L1–GFP, L1 fused to GFP; MSD, mean squared displacement; QD, quantum dot.

L1-family IgCAMs are transmembrane proteins with an ectodomain formed of several FnIII and Ig-like repeats, responsible for parallel and antiparallel associations with a variety of ligands, and a conserved cytoplasmic tail mediating interactions with ankyrin (Tuvia *et al*., 1997), ezrin–radixin–moesin members (Dickson *et al*., 2002), the clathrin adaptor protein AP-2 (Kamiguchi *et al*., 1998b), and postsynaptic density 95/disc-large/zona occludens domain proteins such as syntenin-1 (Koroll *et al*., 2001) and SAP-102 (Davey *et al*., 2005). By modulating these interactions, neurons can regulate the availability of IgCAMs at their surface and the mobility or anchoring of these receptors. For example, the tyrosine phosphorylation-dependent binding of neurofascin/L1 to ankyrin governs its lateral diffusion and coupling to the actin retrograde flow in growth cones (Garver *et al*., 1997; Gil *et al*., 2003; Nishimura *et al*., 2003). Binding of L1 to AP-2 and the clathrin pathway via an YRSLE motif in its cytoplasmic tail enables L1 to be actively recycled in growth cones, being endocytosed in the central domain and exocytosed at the periphery (Kamiguchi and Lemmon, 2000). This mechanism generates a density gradient of L1 molecules that helps growth cones to progress over an L1-coated substrate (Kamiguchi and Yoshihara, 2001).

It is well established that L1 adhesiveness is regulated by trafficking, e.g., reducing L1 exocytosis by tetanus neurotoxin-insensitive vesicle-associated membrane protein (TI-VAMP) silencing leads to impaired binding of L1-coated beads on PC-12 cells (Alberts *et al*., 2003), whereas preventing L1 endocytosis by removing the neuronal RSLE se-

quence promotes L1-dependent cell aggregation (Long *et al*., 2001). However, the actual interplay between L1 molecule trafficking and L1 homophilic adhesion remains unclear. In particular, does the formation of new L1/L1 bonds absolutely require directed exocytosis, or can it simply involve surface receptors that would diffuse randomly on growth cones? Are L1 adhesions at the tip of growth cones more stable than those formed at the rear? How many binding–unbinding events can occur before L1 molecules are endocytosed?

To answer these questions, we mimicked L1-specific contacts by using microspheres coated with purified L1-Fc in contact with neurons transfected with L1-green fluorescent protein (GFP). Using live imaging experiments, we show that L1 adhesions at growth cones form initially via L1 exocytosis and lateral diffusion, accompanied by a coupling to the actin flow. As they mature, L1 contacts continue to recycle through exchange with the membrane pool and endocytosis of L1 molecules.

MATERIALS AND METHODS

GFP-tagged L1 Constructs

For construction of full-length *L1-GFP*, GFP was first amplified by polymerase chain reaction (PCR) from pEGFPC1 (Clontech, Mountain View, CA) by using oligonucleotides inserting a thrombin cleavage site (ctggtaccccgaggatct) at the 3′ end and BamHI sites at each ends. This "GFP–thrombin site" PCR product was purified, digested by BamHI, and inserted into the BamHI site of L1-mouse cDNA (L1–WT in pcDNA3; a kind gift from M. Schachner, Hamburg University, Germany). This resulted in an L1–GFP construct where the N-terminal GFP could be cleaved by extracellular thrombin. For construction of L1 deleted of its intracellular region, L1 was first amplified by PCR from L1-mouse cDNA by using T7 oligonucleotide (upstream start codon) and a designed oligonucleotide (agtcgatatcctagtatttgccacccttgctgcg) inserting a stop codon after the transmembrane domain of L1. The PCR product was cloned by TA cloning, digested by NHEI and EcoRV. The NHEI–EcoRV fragment was subcloned in the NHEI–EcoRI sites of L1–GFP construction. This resulted in a GFP-tagged truncated form of L1 (1153 codons instead of 1259) called *L1-GFPΔCter*. *NrCAM-GFP* where the FnIII domains are replaced by GFP was a gift from J. Falk and C. Faivre Sarrailh (Institut Jean-Roche, Marseille, France) (Falk *et al*., 2004), the original rat neuronal cell adhesion molecule (NrCAM) clone being a gift of V. Bennett (Duke University, Durham, NC). Sequencing of the intracellular region and alignment against the mouse L1 sequence show that NrCAM bears an YSDAE motif in place of the YRSLE internalization motif in L1.

Biochemical Characterization of L1–GFP Proteins

COS-7 cells at a density of 3×10^5/60-mm Petri dishes were transfected with L1–WT, L1–GFP, L1–GFPΔCter, or empty vector by using Lipofectamine (Invitrogen, Carlsbad, CA), and they were cultured in DMEM containing 10% fetal calf serum. After 2 d, cells were rinsed in ice-cold phosphate-buffered saline (PBS), and scraped in TSE buffer (50 mM Tris, pH 8, 150 mM NaCl, 1 mM EDTA, 1% Triton, and cocktail protease inhibitors [Roche Diagnostics, Mannheim, Germany]) after 30 min at 4°C. Lysates were then centrifuged at 13,000 rpm for 20 min, and the supernatant was frozen. Samples were boiled for 5 min in SDS sample buffer and separated on a 4–12% Bis-Tris NuPage gels (Invitrogen). Proteins were transferred onto 0.45-μm nitrocellulose membranes and immunoblotted using rabbit antibodies against the L1 extracellular domain (1/2000; a gift from F. Rathjen, Max-Delbrueck-Center for Molecular Medicine, Berlin, Germany), followed by horseradish peroxidase-conjugated anti-rabbit antibodies (1/10,000; Jackson Immunoresearch Laboratories, West Grove, PA) and developed using the enhanced chemiluminescence method (GE Healthcare, Little Chalfont, Buckinghamshire, United Kingdom).

Production and Purification of L1–Fc

The *L1–Fc* construct composed of the full extracellular domain of L1 fused to the constant fragment of human IgG was a gift from T. Brummendorf (Max-Delbrueck-Center for Molecular Medicine, Berlin, Germany) (De Angelis *et al*., 1999). Human embryonic kidney cells in four flasks of 150 cm^2 were transfected with L1–Fc by using FuGENE (Roche Diagnostics) and cultured for 4 d in DMEM containing 1% Ig-free serum (Sigma-Aldrich, St. Louis, MO). Conditioned medium was collected, filtrated at 0.2 μm, and incubated overnight at 4°C with 500 μl of protein G-Sepharose (GE Healthcare). Beads were rinsed three times in PBS by centrifugation at 2500 rpm for 10 min, and they were placed in a 0.2-μm column (Bio-Rad, Hercules, CA). L1–Fc was eluted for 1 min by using 500 μl of 0.1 M glycine, pH 3.0, and fractions of 240 μl were collected into tubes containing 10 μl of 1 M Tris, pH 9.0, to buffer the pH at 7.2. Protein purity was assessed by gel electrophoresis followed by Coomassie staining, or by immunoblots using mouse anti-Fc (Jackson Laboratories) as a primary antibody. Protein concentration of 150 μg/ml was measured by a protein assay (Bio-Rad) using bovine serum albumin (BSA) (Sigma-Aldrich) as a standard.

Microsphere Coating

Latex microspheres (4-μm sulfate; Interfacial Dynamics Corporation, Tualatin, OR) were coated with goat anti-human Fc or anti-rabbit Fc antibodies (Jackson Immunoresearch Laboratories) by using 10 μg of antibody for 10 μl of the 8% solids bead stock solution (overnight incubation at 4°C in 0.2 M borate buffer, pH 8.5). Beads were rinsed in borate buffer containing 0.3% globulin-free BSA (Sigma-Aldrich), and then they were incubated with 2 μg of L1–Fc, human Fc (Jackson Immunoresearch Laboratories), or 5 μl of rabbit anti-L1 for 3 h at room temperature, rinsed, and resuspended in 100 μl of borate–BSA. Coated beads were kept on ice and used within 8 h.

Neuronal Culture, Transfection, and Incubation with Microspheres

Hipoccampal neurons from embryonic day 18 Sprague-Dawley rat embryos were seeded on 15-mm polylysine-coated glass coverslips at a density of 10,000 cells/cm^2, and they were cultured on a layer of glial cells in Neurobasal medium supplemented with B27 (Invitrogen), as described previously (Goslin *et al*., 1991). Two to 3 d after plating, neurons were transfected with L1–GFP, L1–GFPΔCter, NrCAM–GFP, or GFP by using a phosphate calcium method with 30 μg of DNA for five coverslips (Xia *et al*., 1996), and they were processed 48 h later. Cells were placed in 1 ml of culture medium supplemented with 1% BSA, 20 mM HEPES, and 10 μl of the bead solution, left at 37°C for 0.5 h (except for optical tweezers experiments, where cells were processed immediately), and then rinsed three times in warm medium and mounted in an observation chamber, or fixed for bead counting. When scanning a 15-mm coverslip, one can find an average of 50 transfected cells, representing a transfection efficiency of ~0.5%. This was enough both in immunocytochemistry and live studies to obtain statistically meaningful samples.

Thrombin Treatment

Cells transfected with L1–GFP were treated with 0.1 μM human thrombin (Sigma-Aldrich) at 20 U/ml for 100 s, and then they were rinsed with culture medium containing 50 μM PPACK (Calbiochem, San Diego, CA), a highly selective thrombin inhibitor. This was done just before mounting cells for optical tweezers experiments, or after 0.5-h incubation with microspheres, in which case a perfusion system on the microscope was used in to follow the fluorescence baseline and recovery. Thrombin-treated cells were also allowed to recover up to 2 h, and then they were processed for L1–GFP surface labeling at various time intervals.

Optical Tweezers and Fluorescence Recovery after Photobleaching (FRAP)

The setup combining optical tweezers and FRAP was described previously (Falk *et al*., 2004; Thoumine *et al*., 2006). Briefly, it consists of an inverted microscope (IX 70; Olympus, Tokyo, Japan) fed through its epifluorescence port by a Nd:YAG laser beam (Compass 1064-nm series; Coherent, Santa Clara, CA) and the 488-nm line of an argon laser (Innova 300; Coherent) with appropriate lenses, filter sets, and dichroic mirrors (Chroma Technology, Brattleboro, VT). The laser power at the back of the 100×/1.4 numerical aperture objective is 100 mW for optical trapping and 2.5 mW for photobleaching. Using a motorized stage (MarzHauser, Wetzlar, Germany), microbeads are captured and maintained on neuronal growth cones for 10 s. Images are acquired every 10 s with exposure times of 100–200 ms with a cooled charge-coupled device camera (HQ Cool Snap; Roper Scientific, Tenton, NJ). Using shutters (Uniblitz; Vincent Associates, Rochester, NY), we alternate between bright field and GFP illumination, achieved through a 75-W xenon lamp oriented at a 90° angle and reflected into the epifluorescence port by a infrared dichroic mirror (optical trap) or 70/30 beam splitter (FRAP). The camera and shutters are driven by the MetaMorph software (Molecular Devices, Sunnyvale, CA). For FRAP, a region of interest on a neuron expressing L1–GFP is brought to the position of the laser spot. After acquisition of the baseline level, the sample is bleached for 0.3 s on a 4-μm-diameter area, and fluorescence recovery is recorded for 12 min, with progressively decreasing sampling times. Three optical trapping or FRAP sequences were run at best per coverslip, bringing each experiment duration to ~45 min. Temperature was maintained at 37°C with an air blower (WPI, Sarasota, FL) and an objective heater (Bioptechs, Butler, PA).

Quantum Dot (QD) Labeling and Tracking

One microliter of 655-nm QD conjugated with goat $(Fab')_2$ anti-mouse immunoglobulin (Ig)G (Quantum Dot Corp., Hayward, CA) was incubated with

1 μl of monoclonal anti-GFP (Roche Diagnostics) for 20 min, blocked with 1% casein (Vector Laboratories, Burlingame, CA), and kept on ice for 1–2 d. After binding to microspheres, cells were incubated with the QD suspension (1:10,000) for 5 min in culture medium containing 0.3% BSA, and they were rinsed before mounting on the microscope. QDs were visualized using a 545- to 580-nm excitation filter, 590-nm dichroic mirror, and BA610-nm emission filter (Chroma Technology). Digital images were recorded at a rate of 10 Hz for 100 s. QD positions were tracked using wavelet transform-based multidimensional analysis algorithms included in the MetaMorph software (Racine *et al.*, 2006), and trajectories were reconnected using routines written in the MathLab software (MathWorks, Natick, MA) described previously (Tardin *et al.*, 2003). Traces longer than 6 s were selected. The mean squared displacement was calculated for each trajectory and fit by linear regression on the first 3 s, giving an instantaneous diffusion coefficient.

Immunocytochemistry

For staining of total endogenous L1 or L1–GFP, cells were fixed for 10 min in warm 4% paraformaldehyde–4% sucrose in PBS, and the remaining active sites were saturated with 50 mM NH_4Cl in PBS for 15 min. Cells were permeabilized with 0.3% Triton X-100 in PBS for 5 min, and nonspecific binding sites were blocked with 1% BSA in PBS for 30 min. Cells were incubated in PBS–BSA with 1:400 rabbit anti-GFP (Invitrogen) or 1:100 anti-L1 for 2 h, rinsed extensively, and incubated with 1:800 Alexa 568-conjugated goat anti-rabbit antibody (2 mg/ml; Invitrogen) for 1 h, and mounted in Vectashield (Vector Laboratories). To estimate the amount of endogenous L1 in nontransfected cells, we subtracted the staining obtained with the secondary antibody alone from the anti-L1 staining (Supplemental Figure 1).

To estimate the proportion of surface versus intracellular L1 molecules, L1–GFP-transfected cells were labeled using 1:400 rabbit anti-GFP as a primary antibody under permeabilized or nonpermeabilized conditions, respectively, and the fluorescent signals on growth cones were compared. For surface staining, neurons transfected for L1–GFP were incubated in 50 μl of culture medium containing 1% BSA and 1 μl of monoclonal anti-GFP (Roche) for 10 min at room temperature. The neurons were then rinsed and processed as described above without the permeabilization step.

For assessment of endocytosed receptors, neurons transfected with L1–GFP, L1–GFPΔCter, or NrCAM–GFP (comparisons made on the same batches) were incubated with 1:50 monoclonal anti-GFP at 4°C for 5 min. The cold condition is used to avoid massive internalization of primary antibody complexes during the labeling period. Cells were then fixed immediately with paraformaldehyde or placed at 37°C for 15 min, allowing endocytosis to proceed. L1–GFP molecules remaining at the cell surface were efficiently blocked with a mixture of 1:20 unconjugated goat anti-mouse Fc (2 mg/ml; Jackson Immunoresearch Laboratories) and 1:20 Alexa 350-conjugated (irrelevant fluorophore) goat antibodies against both heavy and light chains mouse IgG (Invitrogen). Cells were permeabilized with 0.1% Triton X-100 for 1 min before labeling with 1:800 Alexa 568-conjugated anti-mouse antibody. We selected neurons with intermediate L1–GFP expression levels, and we took images of the L1–GFP fluorescence and the anti-GFP immunostaining with constant exposure times. The Alexa 568/anti-GFP signal was then divided by the corresponding L1–GFP signal on the same growth cones, and the ratio was averaged.

RESULTS

Surface Expression and Exocytosis of L1–GFP Molecules

To distinguish L1 molecules expressed at the cell surface from the internal pool, we fused the GFP sequence to the N terminus of the full-length mouse L1 gene (*L1-GFP*), by using a linker that can be cleaved with thrombin. We also produced an L1–GFP receptor deleted of the intracellular domain, *L1-GFPΔCter* (Figure 1A), to abolish interactions with the cytoskeleton and the endocytotic pathway. Expres-

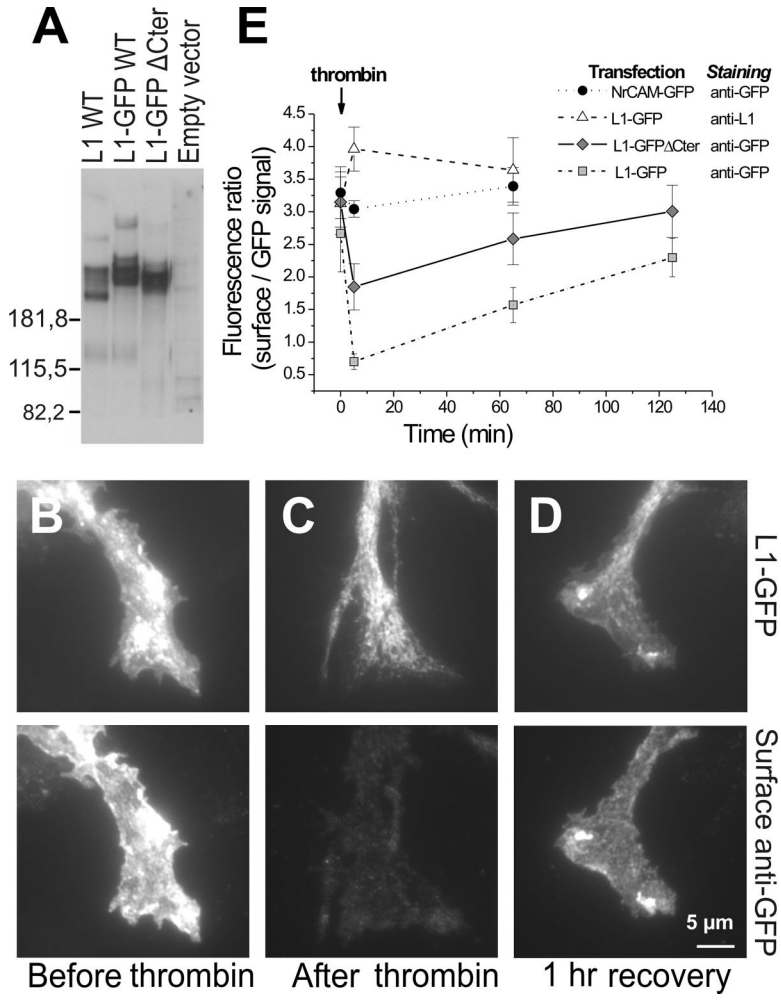

Figure 1. Biochemical characterization and distribution of L1–GFP fusion proteins. (A) L1–WT, L1–GFP, L1–GFPΔCter, or the empty vector were transfected into COS cells, and cell lysates were processed for immunoblotting with anti-L1. Note the shift in molecular weight between the various constructs and the absence of nonspecific staining. Neurons transfected for L1–GFP, L1–GFPΔCter, or NrCAM–GFP were treated with thrombin for 100 s, and then they were rinsed and allowed to recover for selected time intervals. Cells were then incubated live with anti-GFP or anti-L1 antibodies for 5 min, fixed, and stained with secondary antibodies conjugated to Alexa 568. (B–D) Representative images of growth cones from cells transfected for L1–GFP (top) and surface stained with anti-GFP (bottom), before (B), right after (C), or 1 h after (D) thrombin treatment. (E) Time course of surface fluorescence recovery after thrombin treatment at time zero, for all conditions. Data are expressed as the average ± SEM of the ratio of Alexa 568/GFP signal for at least 10 growth cones in each condition. Linear regressions through the data give the basal export rates of L1 molecules to the growth cone surface (0.012 and 0.0097 min^{-1} for L1–GFP and L1–GFPΔCter, respectively).

sion of both constructs in COS cells yielded protein products at the expected molecular weights ~200 kDa (Figure 1A). When transfected into rat hippocampal neurons at 3–4 d in vitro (DIV), L1–GFP molecules were distributed at the growth cone surface, and they also were present intracellularly at the base of growth cones (Figure 1B). L1–GFP was also expressed at high levels within the cell body, in a perinuclear area likely corresponding to the synthesis and secretion pathway (Supplemental Figure 1B). By comparing detergent-permeabilized and non-permeabilized L1–GFP-expressing cells immunostained with anti-GFP antibodies, we estimated that 43 ± 9% of L1-GFP (n = 16 cells) and 23 ± 3% of L1-GFPΔCter (n = 10) at growth cones were surface associated. By comparing L1–GFP-positive cells to nontransfected counterparts both immunostained with anti-L1 antibodies (Supplemental Figure 1), we estimate that the ratio of exogenous L1–GFP protein to that of endogenous L1 is 5 ± 1 at the surface (n = 10 cells). Such overexpression does not perturb the correct targeting and axonal compartmentalization of NgCAM, the chick homologue of L1, in the same cultures (Sampo *et al*., 2003; Wisco *et al*., 2003).

To evaluate the rate and spatial distribution of L1 exocytosis, L1–GFP-transfected neurons were briefly treated with thrombin to cleave the GFP-tag of surface L1–GFP molecules, and then the neurons were allowed to recover. We observed an immediate 80% loss of surface staining (Figure 1, C and E), with a simultaneous 40% decrease in L1–GFP signal preferentially from the lamellipodium. The 60% leftover was mainly due to the presence of intracellular L1–GFP in the central domain (Figure 1C). Anti-GFP surface staining came back to baseline in several hours with a characteristic rate on the order of 0.01 min^{-1} (Figure 1, D and E), revealing a progressive exocytosis of L1–GFP. An enrichment of newly exported L1–GFP molecules at the periphery of growth cones, especially in ruffles, was sometimes observed (Figure 1D). Thrombin acted specifically, because it affected neither the distribution of surface L1 nor that of NrCAM bearing a noncleavable GFP-tag (Figure 1E). Although hippocampal neurons express thrombin receptors (Yang *et al*., 1997), thrombin can induce significant effects only when applied at much higher concentrations and for longer times than the times used here (Brewer, 1996; Donovan *et al*., 1997). Indeed, thrombin did not alter growth cone motility or cause neurite retraction in our conditions (Figure 5). The L1–GFPΔCter mutant was slightly less expressed at the cell surface than wild-type L1, as reflected by a less efficient thrombin cleavage, but it showed a similar export dynamics to the growth cone surface (Figure 1E). This agrees with the finding that mutated NgCAM molecules go to the axonal surface even in the absence of interactions with intracellular partners (Boiko *et al*., 2007).

Intracellular L1 Molecules Undergo Polarized Trafficking in Growth Cones

We further used thrombin to enhance the visualization of internal L1–GFP-rich vesicles in growth cones. Most vesicles were stuck at the base of growth cones, with undetectable motion (Figure 2, A and B, arrowheads). However, we also

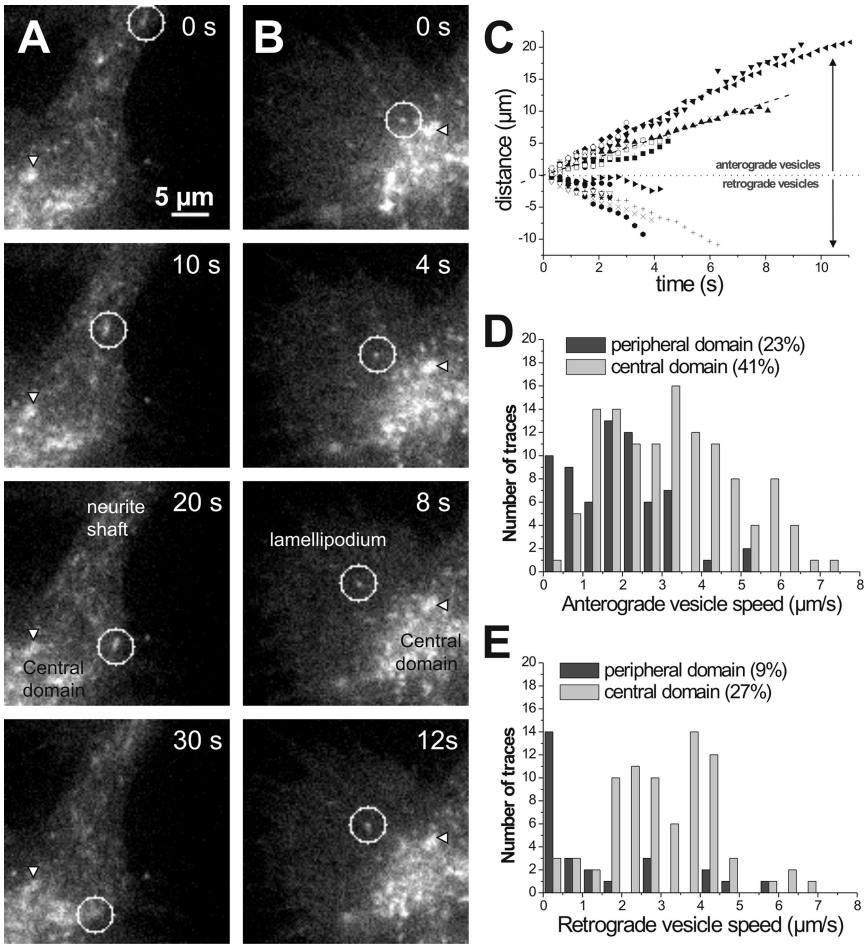

Figure 2. Directed motion of L1–GFP-rich vesicles within growth cones. Neurons transfected with L1–GFP were treated with thrombin for 100 s, and then they were rinsed and observed under the microscope. The distribution of intracellular L1–GFP fluorescence within growth cones was filmed at a rate of three to five images per second. The majority of L1–GFP-rich vesicles stayed confined at the base of the growth cone (arrowheads). (A and B) Representative examples of two vesicles moving forward on the same growth cone (circles), one in the neurite shaft (A) and the other in the lamellipodium (B). (C) The position of such vesicles was tracked, and their displacement was plotted over time. The relationship was fairly linear, the slope of which being taken as the vesicle velocity. The velocity of both anterograde (D) and retrograde (E) moving vesicles was computed, and it is plotted as histograms. By applying an intensity threshold on the L1–GFP fluorescence image, we distinguished a rather uniform less intense zone at the periphery of growth cones (the peripheral domain), and a more intense zone rich in L1-GFP vesicles at the base of growth cones (the central domain). Moving vesicles are classified according to their presence in either of these two areas (black and gray bars, respectively).

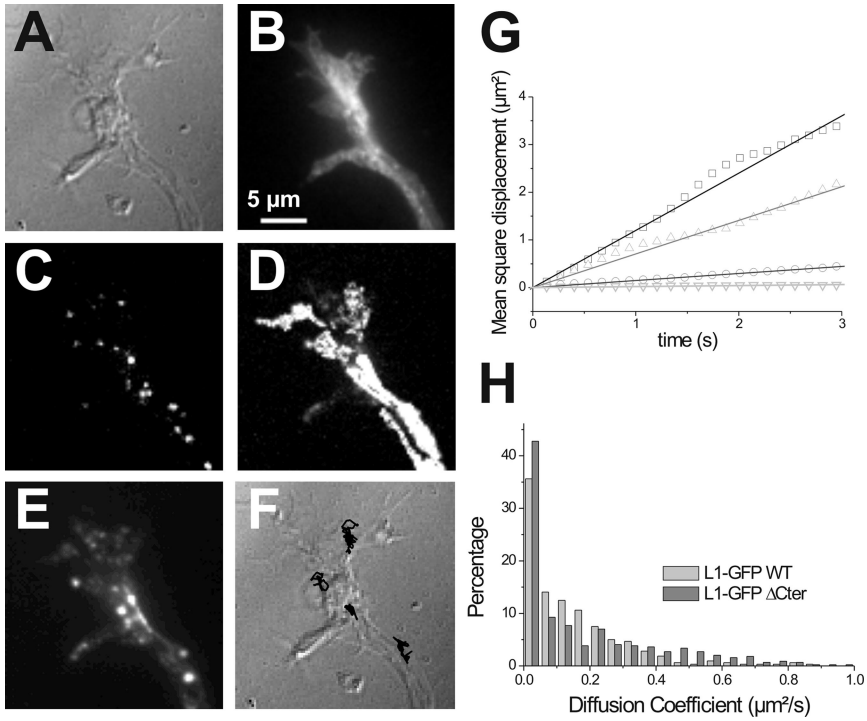

Figure 3. Random diffusion of individual L1–GFP molecules at the growth cone surface. Neurons transfected for L1–GFP or L1–GFPΔCter were labeled with anti-GFP–coated quantum dots. (A) Differential interference contrast (DIC) image. (B) L1–GFP image. (C) Instantaneous image of QDs bound to the growth cone. (D) Image of the maximum intensity from the QD channel detected for each pixel integrated along a 1-min sequence, representing the global area explored by QD. (E) Image of the average intensity from the QD channel detected for each pixel along a 1-min sequence, representing the preferential zones of QD immobilization. (F) Examples of four trajectories superimposed on the DIC image. (G) Mean squared displacement versus time for typical trajectories, from immobile to very mobile. The linear fits give the corresponding diffusion coefficients. (H) Histogram of the diffusion coefficients for L1–GFP and L1–GFPΔCter computed from 537 and 688 traces, respectively.

observed the rapid and highly directed movement of L1–GFP-rich vesicles, in either the retrograde or anterograde directions (Figure 2, A and B, circles). Vesicles were found to move at high speed along neurites and into the central area (Figure 2A), whereas those in the lamellipodium moved more slowly (Figure 2B). Overall, there was a preference for anterograde motion (64% of vesicles) versus retrograde motion (36%), especially in the growth cone lamellipodium (27 vs. 9%, respectively), indicating a selective transport of L1-rich vesicles toward the growth cone periphery (Figure 2D). Indeed, we sometimes saw vesicles originating from the base of growth cones and disappearing at their periphery, possibly by fusion with the plasma membrane (Supplemental Movie 1). Vesicles in the neurite shaft and central domain moved at the same speed in both anterograde and retrograde directions, with an average velocity of 3 μm/s (Figure 2, D and E), which compares well with that of microtubule motors. Furthermore, the very straight trajectories (Figure 2C) suggest that these L1–GFP vesicles are transported along dynamic microtubules, which have been reported to invade the growth cone lamellipodium (Dent and Gertler, 2003). Indeed, in the presence of the microtubule-depolymerizing drug nocodazole, vesicles seemed to exhibit higher Brownian diffusion, and very few adopted a directed movement (data not shown). Regardless of the direction, vesicles moved more slowly in the lamellipodium than in the neurite shaft, with average velocity around 1 μm/s close to that reported for FM1-43 loaded or VAMP-2–containing vesicles toward the growth cone peripheral domain in dorsal root ganglion (DRG) neurons (Tojima *et al*., 2007). This suggested a different transport mechanism or a steric difficulty to progress through a dense actin network moving backward. In support of the latter hypothesis, treatment with the actin-depolymerizing drug cytochalasin D accelerated vesicle motion (Supplemental Movie 2). We observed similar velocities for L1–GFP and L1–GFPΔCter, further indicating that this mutant underwent normal export. We next assessed whether this polarized trafficking of L1 was also present at the cell surface.

L1 Molecules Diffuse Randomly on the Growth Cone Surface

To visualize the lateral motion of plasma membrane L1 molecules, we labeled a subset of surface-associated L1–GFP molecules by using anti-GFP-coated QDs (Supplemental Movie 3). QDs bound exclusively to transfected neurons, and they moved over the growth cone area (Figure 3, A–E). Their trajectories were automatically tracked (Figure 3F) and analyzed by calculation of the mean squared displacement (MSD) over time (Figure 3G). The MSD was fairly linear over time, indicating a predominance of Brownian motion. This was in agreement with a recent study showing that neurofascin diffuses randomly in the distal axon at a similar developmental stage (4 DIV) (Boiko *et al*., 2007). We never observed any clear directionality, which would occur as a parabolic MSD (Sheetz *et al*., 1990). As a global estimation of lateral mobility, we quantified the instantaneous diffusion coefficient of individual trajectories, taken as the slope of the MSD (Figure 3H). Because of the heterogeneity of behaviors, the data show up as a distribution of diffusion coefficients (Figure 3G). The average value for L1–GFP was 0.25 $\pm$ 0.01 μm^2/s (n = 537 trajectories), slightly greater than the value reported for neurofascin by using 1-μm latex beads, likely owing to probe size (Boiko *et al*., 2007). The distribution for the L1ΔCter mutant was shifted to higher diffusion values, with a mean diffusion coefficient of 0.29 $\pm$ 0.01 μm^2/s (n = 689 trajectories). Setting a threshold of 0.05 μm^2/s, we defined an immobile fraction which reaches 30% for L1–GFP and 40% for L1–GFPΔcter. A fraction of immobile QDs (roughly 50%) was distributed at the base of growth cones (Figure 3E) and partially colocalized with clathrin-DsRed clusters (data not shown), suggesting that they were associated with endocytotic compartments. However, the colocalization of immobile QD with clathrin-coated pits was not

total, because QDs may sterically restrict the accessibility of L1–GFP to these compartments, or because L1–GFP molecules are trapped in other compartments (e.g., by interaction with immobile cytoskeletal components).

L1–Fc and Anti-L1–coated Microspheres Adhere Specifically to L1-expressing Neurons

We then assessed the relative contributions of these two apparently coexisting pathways, i.e., directed exocytosis versus membrane diffusion, in the formation of nascent L1-dependent adhesions. To create L1-specific contacts, we purified a recombinant L1–Fc molecule made of the extracellular domain of L1 fused with human Fc (Figure 4C). We also used antibodies against the extracellular domain of L1 as a positive control, and human Fc alone as a negative control. Microspheres coated with L1–Fc but not with human Fc adhered stably to the surface of untransfected cells, indicating adhesion specificity (Figure 4, A and B). Beads coated with anti-L1 also adhered strongly, revealing the presence of endogenous L1. Neurons transfected with L1–GFP bound ~2 times more L1–Fc and anti-L1–coated microspheres than untransfected cells or cells transfected with GFP alone (Figure 4, A and B), indicating that the L1–GFP protein was expressed at the cell surface and could form homophilic interactions with L1–Fc ligands. Moreover, both anti-L1–coated and L1–Fc-coated microspheres recruited L1–GFP molecules (Figure 4A). Only a fraction of microspheres (roughly 30%) showed significant accumulation of L1–GFP molecules: this heterogeneity may reflect variability in L1–Fc ligand coating or availability of L1–GFP molecules. For example, beads at the cell body generally recruited less L1–GFP than at the growth cones (Figure 4A), possibly owing to, respectively, a lower concentration of L1–GFP at the cell surface (Supplemental Figure 1C) or a reduced binding due to a lack of selective L1–GFP export (see next paragraph). We quantified an enrichment factor as the fluorescence level within bead contacts divided by the control level on adjacent regions, which reaches a value of ~2 at equilibrium.

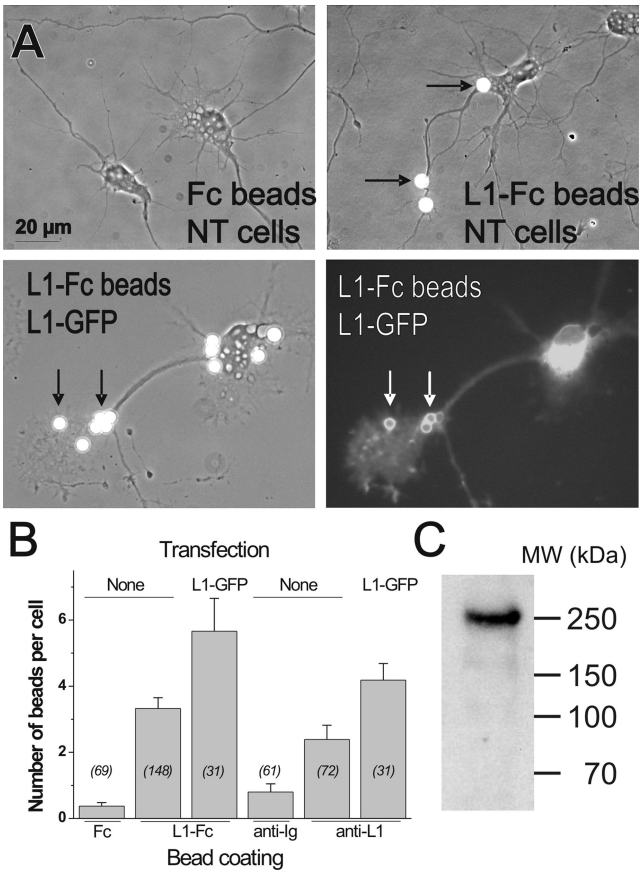

Figure 4. Specific binding of L1–Fc and anti-L1–coated microspheres to neurons. (A) Untransfected neurons (NT) or neurons transfected for L1–GFP were incubated for 0.5 h with latex microspheres coated with human Fc, L1–Fc, or anti-L1 antibodies, and then they were rinsed and fixed. Note the accumulation of L1–GFP fluorescence around L1–Fc- or anti-L1–coated microspheres (white arrows). (B) The number of beads bound per cell in each condition is expressed as mean ± SEM, with the number of cells examined in italics. (C) The purified L1–Fc protein was run on a polyacrylamide gel and immunoblotted with antibodies against L1, showing migration at the expected molecular weight.

The Early Accumulation of L1 at Adhesive Contacts Partially Relies on Exocytosis

To probe the early phase of L1–GFP accumulation at adhesive contacts, we placed L1–Fc- or anti-L1–coated microspheres on motile growth cones with optical tweezers, and we monitored the redistribution of L1–GFP by fluorescence imaging (Supplemental Movie 4). As a negative control, we used microspheres coated with N-cadherin-Fc (Thoumine *et al*., 2006). Beads adhered firmly and started to move rearward, and then they slowed down as they reached the base of the growth cones (Figure 5, A and B). The initial retrograde velocity (4 μm/min) was relatively independent of ligand coating (Figure 5E). That velocity corresponded closely to the actin flow rate (Diefenbach *et al*., 2002), suggesting that beads were coupled to the actin cytoskeleton. Meanwhile, we observed a progressive accumulation of L1–GFP fluorescence around L1–Fc- and anti-L1–coated beads, reaching a plateau in a few minutes, whereas microspheres coated with N-cadherin accumulated significantly less signal (Figure 5C). The instantaneous enrichment factor was fit by an equation derived from first-order chemical kinetics (Figure 5C), giving a characteristic accumulation rate in units of minutes^{-1} (Table 1). The rates of L1–GFP accumulation at L1–Fc beads was, respectively, 4 and 14 times larger than for microspheres coated with anti-L1 or anti-GFP antibodies (Table 1). This demonstrated high ligand specificity in the recruitment of L1 molecules, with L1–Fc likely inducing stronger activation than nonperturbing antibodies.

To determine the compartments (surface vs. intracellular) involved in such accumulation of L1 molecules around microspheres, cells were pretreated with thrombin for 1 min before placing the microspheres on growth cones, to initially remove surface fluorescence. We still observed a notable accumulation of L1–GFP around beads coated with L1–Fc and anti-L1 antibodies, indicating a significant contribution from newly exocytosed L1–GFP molecules. Normalization of the L1–GFP signal at bead contacts by a control level on the same growth cone (enrichment factor) compensates for photobleaching and/or basal increase in L1-GFP outside bead contacts and measures the true accumulation of L1-GFP on the bead surface. Given the relatively large diameter of the bead (4 μm) with respect to the size of the growth cone (10–15 μm), we cannot tell with precision whether exocytosis occurs directly at the bead contact or nearby, followed by fast diffusion. However, in the continuous presence of thrombin, we occasionally observed the sudden disappearance of vesicles at L1–Fc microspheres, suggesting that they were fusing with the plasma membrane directly at the bead

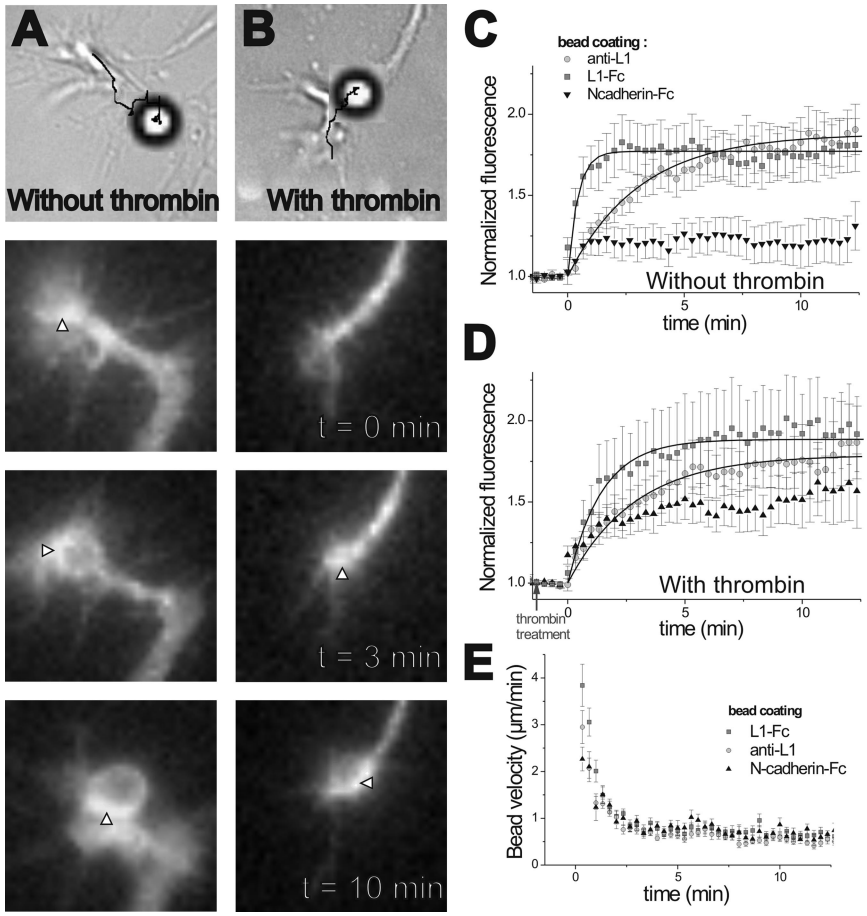

Figure 5. Microspheres move rearward on growth cones and progressively accumulate L1–GFP molecules. Microspheres coated with L1–Fc, Ncad–Fc, or antibodies against L1 were placed for 10 s at the periphery of growth cones from L1–GFP-transfected neurons, by using an optical trap. (A and B) The movement of the bead and the fluorescence accumulation at the bead contact (arrowheads) were followed for 10 min. The black trace on the white field upper image indicates the bead trajectory, and the bead position is shown at the end of the experiment (for better contrast, we superimposed the white field image of the bead to a DIC image of the growth cone obtained at the end of the sequence). Cells were either left untreated (A) or pretreated with thrombin for 1 min, and then they were rinsed in the presence of PPACK before optical tweezers manipulation (B). The fluorescence level around the bead was normalized by that on adjacent regions and plotted over time for untreated cells (C) or cells pretreated with thrombin (D). Data are expressed as mean ± SEM, and they are fit with a first-order kinetics model (plain curves) (Thoumine *et al*., 2006). (E) The instantaneous bead velocity is plotted over time for the different bead coatings, pooling data from conditions with or without thrombin, which did not differ in terms of velocity. The number of experiments (between 10 and 20) is given in Table 1.

contact (Supplemental Movie 6). Control beads coated with Ncad–Fc exhibited some residual accumulation in L1–GFP after initial thrombin treatment (Figure 5D), due to the fact that microspheres were progressively reaching the base of growth cones rich in L1–GFP vesicles. These experiments represent the nonspecific component, and fitting the data would give recruitment rates that are not meaningful.

The steady-state fluorescence accumulation was similar in the absence and presence of thrombin, but we cannot directly compare these equilibrium values because the normalization is based on a different internal control for each condition (total vs. intracellular receptors outside bead contacts). More informative are the accumulation rates. Indeed, L1–GFP molecules accumulated approximately twofold slower at L1–Fc beads in the presence of thrombin but still much faster than the baseline export rate outside bead contacts (Table 1), indicating preferential exocytosis at L1–Fc adhesions. The effect was less pronounced for anti-L1–coated beads (Table 1), suggesting some ligand specificity in this export of L1 molecules. If one considers membrane diffusion and trafficking as two parallel pathways, the overall accumulation rate in the absence of thrombin should be the sum of that due to exocytosis (in the presence of thrombin) and that due to lateral motion. We can thus deduce that lateral diffusion

Table 1. Rates of accumulation of L1–GFP molecules at L1–Fc, anti-L1–, or anti-GFP–coated microspheres, in the presence (+) or absence (−) of initial thrombin cleavage

	Thrombin cleavage					
	−	−	−	+	+	+
Ligand	L1–Fc	Anti-L1	Anti-GFP	L1–Fc	Anti-L1	No bead
k_{on} (min^{-1})	1.30 ± 0.35	0.32 ± 0.05**	0.09 ± 0.02****	0.63 ± 0.09*	0.23 ± 0.05	0.012
n	17	19	13	11	13	NA

The data for anti-GFP beads is taken from Thoumine *et al.* (2005). The rate for the no bead condition is calculated from immunostaining of surface anti-GFP after thrombin cleavage (see Figure 1E), from which we could not calculate a variance. Data are expressed as mean ± SEM, with n representing the number of beads. NA, not applicable. Rates were found to be statistically different by ANOVA and compared with the L1–Fc condition without thrombin by Tukey's test (*$p < 0.05$; **$p < 0.01$; ****$p < 0.001$).

and exocytosis contribute equally to L1 molecule recruitment at L1–Fc contacts.

L1 Molecule Exocytosis Does Not Occur at Mature L1 Adhesions

To assess whether exocytosis was also occurring in stable L1-based adhesions, we incubated L1–GFP-transfected neurons with L1–Fc and anti-L1–coated beads for 0.5 h. We then selected areas with beads showing L1–GFP accumulation, perfused cells with thrombin for 1 min, and monitored L1–GFP distribution at bead contacts after washing (Figure 6A and Supplemental Movie 6). Treatment with thrombin caused a rapid 60% drop of fluorescence signal around beads, corresponding to the cleavage of the GFP-tag on L1–GFP-associated with beads at the cell surface (Figure 6B). After washing, the fluorescence at bead contacts recovered very slowly for both types of beads, revealing almost no detectable exocytosis of L1–GFP molecules. We took care to image at a sufficiently slow rate and with high pixel binning so as to cause minimal photobleaching during image acquisition. Furthermore, the lack of recovery was not due to the presence of persistent thrombin, because we added in the washing buffer a highly selective thrombin inhibitor (PPACK), which totally blocks the GFP cleavage (Figure 6B). Thus, L1 molecules are no longer exocytosed at stable L1-contact sites. This begged the question of whether receptor recycling could still occur in mature L1 adhesions.

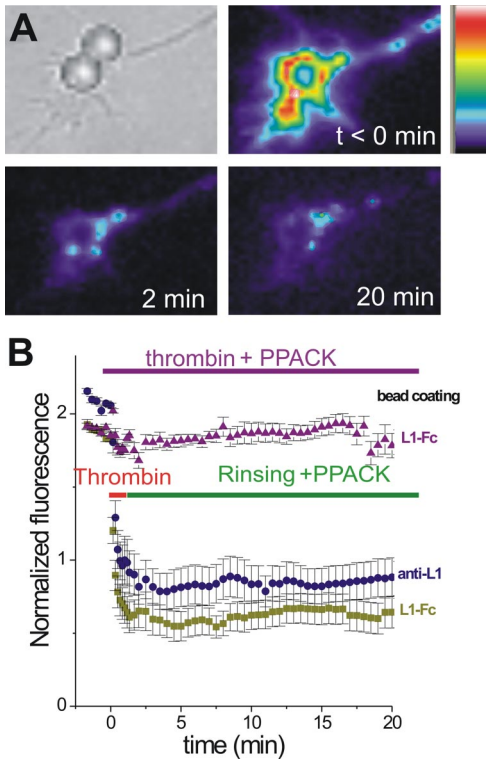

Figure 6. Lack of fluorescence recovery at L1–GFP-rich contacts after GFP cleavage by thrombin. (A) Neurons transfected for L1–GFP were incubated for 0.5 h with anti-L1– or L1–Fc-coated microspheres, leading to fluorescence accumulation around beads. Cells were treated with thrombin for 100 s, resulting in a dramatic decrease in fluorescence around beads, and then they were rinsed with fresh buffer containing a highly selective thrombin inhibitor (PPACK) and imaged for 20 min. (B) The enrichment factor (bead/control area) is plotted over time for L1–Fc and anti-L1 beads, thrombin being applied at time 0. In some experiments (triangles), cells were treated with thrombin + PPACK for 20 min. Data from 15 to 18 individual beads are expressed as mean ± SEM.

At Equilibrium, L1/L1 but Not Anti-L1/L1 Adhesions Quickly Turnover

To investigate whether stable L1-dependent adhesions where capable of turnover, we allowed L1–Fc or anti-L1–coated beads to stay in contact with neurons for 0.5 h, leading to equilibrium accumulation of L1–GFP around beads. The enrichment factor was, respectively, 1.8 and 2 for L1–Fc and anti-L1–coated beads, corresponding well to the steady-state values obtained from recruitment experiments (Figure 5C). We then selectively photobleached bead-to-cell contacts by using a defocused laser spot precisely matching the bead diameter, and we measured the fluorescence recovery in the same bead area (Figure 7A), a protocol previously used to estimate N-cadherin recycling rates (Thoumine *et al*., 2006). We compared these experiments with similar control recordings performed on neurites or growth cones (no bead). The difference between the two conditions (bead vs. no bead) is expected to reflect the specific behavior of bound receptors at the bead contact. Indeed, for L1–Fc beads the signal increased in two steps (Figure 7B): 1) a rapid phase during the first 2 min, superimposable to the no-bead condition, likely reflecting the diffusion of unbound and intracellular receptors; and 2) a slower phase reaching higher levels than on control areas (1.3 in 12 min), indicating that bleached L1–GFP molecules initially trapped by the L1–Fc-coated beads were progressively replaced by fresh L1–GFP. The data were fitted by a diffusion-reaction model (Thoumine *et al*., 2006), allowing the characterization of the equilibrium turnover rate of L1–L1 homophilic bonds (Table 2). In contrast, the second recovery phase was almost absent for beads coated with anti-L1 antibodies (Figure 7B), which exhibited fourfold lower turnover rates attributed to the intrinsic stability of antibody–antigen bonds (Table 2). A similar behavior was observed for microspheres coated with anti-GFP antibodies (data not shown). Thus, there is a selective turnover of L1–L1 adhesions at equilibrium.

Endocytosis Is Involved in the Turnover of Stable L1–L1 Adhesions

We finally asked the question of whether endocytosis could be implicated in the turnover of mature L1 adhesions. For this, we made an L1–GFP construct deleted of its intracellular domain, to prevent interactions with the endocytotic pathway (Kamiguchi *et al*., 1998b). The L1–GFPΔCter protein, which carries the proper signal peptide, was correctly addressed to the cell surface (Figure 8, A and B), and it was recruited around L1–Fc-coated microspheres (enrichment factor = 1.9 ± 0.1; n = 20 beads), showing that it retained homophilic binding activity, as reported previously (Wong *et al*., 1995). Using an antibody feeding assay, we compared the endocytosis of L1–GFP and L1–GFPΔCter molecules. After a 15-min internalization period, the typical time course of a FRAP experiment, newly endocytosed L1–GFP molecules were found as discrete spots localizing mainly in the central region of the growth cone (Figure 8, C and D). There was a significant 30% decrease in the internalization of L1–GFPΔCter molecules in this region, compared with wild-type L1–GFP molecules (Figure 8, C–E).

We then carried out FRAP experiments using the L1–GFPΔCter construct at L1–Fc bead contacts (Figure 7C). L1–GFPΔCter molecules recycled approximately threefold more slowly than wild-type counterparts (Table 2). This effect may implicate differences in lateral mobility, surface expression, or endocytosis rate, which all potentially con-

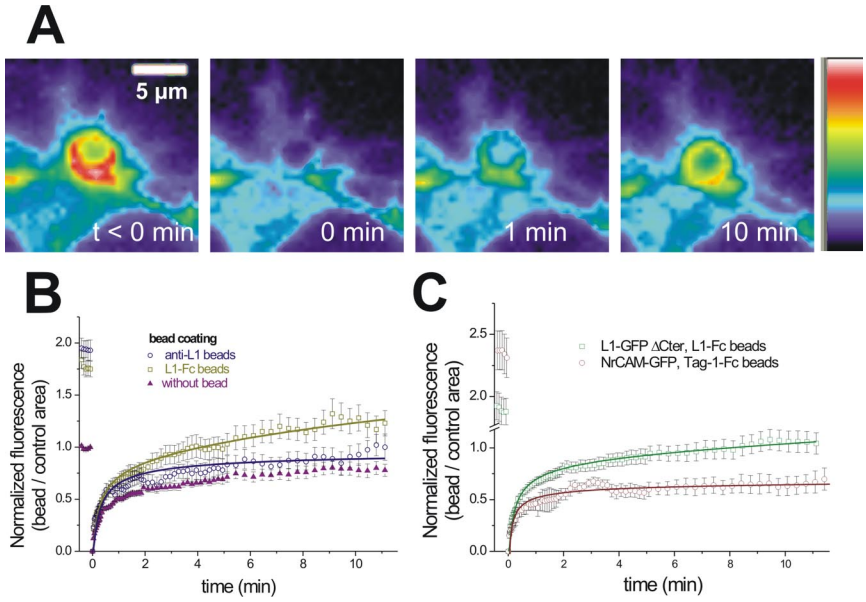

Figure 7. Rapid turnover of L1 molecules within L1–Fc bead contacts at equilibrium. Neurons transfected for L1–GFP or L1–GFPΔCter were incubated for 0.5 h with anti-L1– or L1–Fc-coated microspheres, which recruited L1–GFP up to saturation. The L1–GFP signal on microspheres or on adjacent regions was photobleached at time 0, and the recovery of fluorescence was followed for 12 min. (A) Time sequence of a typical FRAP experiment. (B) Normalized enrichment factor over time. Data are expressed as mean ± SEM, and the plain curves are fits with a diffusion-reaction model (Thoumine *et al.*, 2006). In this analysis, we continue using the enrichment factor (ratio bead/control area), starting with a prebleach value of ~1.8, and reason essentially on the 80% fraction representing the L1–GFP specifically accumulated at the bead surface. When we photobleach the whole L1–GFP signal at a bead contact, we bleach the 100% fraction, which behaves like L1–GFP outside the bead contact (intracellular + unbound molecules), and which recovers rapidly (no bead curve). We simultaneously bleach the 80% L1–GFP molecules associated with the bead contact, and this fraction recovers more slowly (second regime) for L1–Fc beads. In the case of anti-L1 beads, it does not recover at all, the anti-L1 curve staying at the same level as the "no bead" condition. This demonstrates that these receptors are permanently immobilized by antibodies on the cell surface. (C) FRAP curves for L1–GFPΔCter at L1–Fc contacts in hippocampal neurons and NrCAM-GFP at TAG-1 bead contacts in B104 neuroblastoma cells. The turnover rates calculated from the model are given in Table 2 with the corresponding number of experiments.

tribute to the recycling of L1 adhesions. The fact that L1-GFPΔCter shows increased surface diffusion should increase the L1–GFPΔCter renewal rate and not the contrary. In addition, the lower availability of L1–GFPΔCter mutant at the cell surface should accelerate the adhesion turnover rate, by displacing the ligand–receptor binding reaction toward faster dissociation. Thus, the reduced endocytosis of L1–GFPΔCter caused by a lack of interaction with the endocytotic pathway may be the primary mechanism of its reduced turnover rate at L1–Fc contacts. The fact that the modest 30% decrease in endocytosis rate for L1–GFPΔCter measured outside bead contacts is paralleled by a threefold decrease in turnover rate suggests a nonlinear response, in which L1 molecules trapped at L1–Fc microspheres, could undergo higher endocytosis than free molecules, as reported to occur for ligand-bound L1 in a phosphorylation-dependent manner (Schaefer *et al.*, 2002). Internalization would then represent a driving force that promotes unbinding by making L1 molecules selectively disappear from the membrane.

To further examine the role of L1 endocytosis in adhesion turnover and establish the specificity of the L1–L1 interaction in comparison to other IgCAMs, we used an NrCAM–GFP construct, which shows high homology to L1 in the intracellular domain except that it bears an YSDAE sequence in place of the YRSLE AP-2 binding motif (Falk *et al.*, 2004). NrCAM–GFP was indeed less internalized than both L1–GFP and L1–GFPΔCter (Figure 8C). We also measured the adhesion turnover rate of NrCAM–GFP by reanalyzing previous FRAP experiments using TAG-1–Fc coated beads (Falk *et al.*, 2004). TAG-1 is a member of the IgCAM family showing homology with the L1 extracellular domain, and it is a natural ligand for NrCAM. We monitored a complete absence of recycling of NrCAM–GFP at TAG-1–Fc bead contacts (Figure 7C and Table 2). Although a possible difference in affinity between the NrCAM–TAG-1 and L1–L1 interactions may also affect turnover rate, this finding represents a strong evidence for the implication of endocytosis in the recycling of L1 adhesions.

DISCUSSION

Validation of the Experimental System

Mutations in the L1 gene that impair L1 homophilic adhesion are associated with severe brain pathologies in humans (De Angelis *et al.*, 1999), hydrocephalus in certain strains of knockin mice (Itoh *et al.*, 2004), and misplacement of neurons in *Caenorhabditis elegans* (Sasakura *et al.*, 2005). Thus, considering the importance of L1 adhesion in axonal migration and targeting (Kamiguchi *et al.*, 1998a; Brummendorf and Lemmon, 2001), we focused here on the dynamics of L1–L1 interactions in the growth cone. We cultured primary hippocampal neurons, and we transfected them with L1–GFP to monitor L1 molecule redistribution in various assays. L1 is detectable as mRNA in the hippocampus (Horinouchi *et al.*, 2005), whereas there are contrasting results concerning the presence of L1 protein (Miller *et al.*, 1993; Munakata *et al.*, 2003), probably depending on antibody reactivity, staining protocols, or mouse strains. Nevertheless, L1 plays a functional role in this brain region (Itoh *et al.*, 2005). L1–GFP molecules were correctly expressed at the cell surface, and they could be endocytosed and exocytosed with rates similar to those measured previously in DRG neurons by using pulse-chase experiments with antibodies against endogenous L1 (Kamiguchi and Lemmon, 2000), revealing the functionality of the L1–GFP protein. We mimicked L1-specific contacts by using microspheres coated with L1–Fc or anti-L1 antibodies, allowing a precise control of the type of ligands presented to neurons and of the initial time of the interaction (Pollerberg *et al.*, 1990). We confirmed that the turnover rates we measured on microspheres correlated well with those obtained for spontaneous neuronal adhesions formed in slightly older cultures (Supplemental Figure 3). L1–GFP ac-

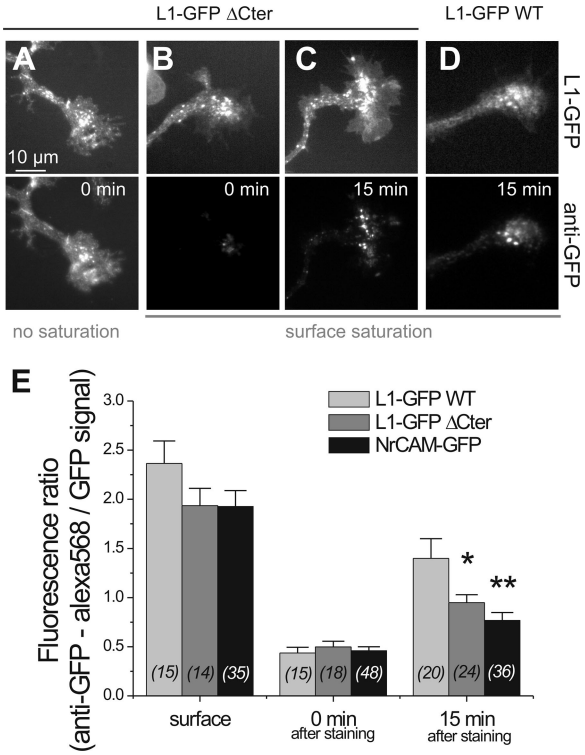

Figure 8. Endocytosis of L1 at the base of growth cones. (A–D) Neurons transfected for L1–GFP, L1–GFPΔCter, or NrCAM–GFP were briefly fed with soluble antibody against GFP, and then they were either fixed immediately (A and B) or placed at 37°C for 15 min to promote internalization of receptor–antibody complexes (C and D). (A) Surface anti-GFP–labeled receptors were stained with fluorescent secondary antibody without cell permeabilization. (B–D) Surface labeling was quenched by high concentrations of unconjugated secondary antibody, and internalized L1–GFP molecules were labeled with fluorescent secondary antibody after brief permeabilization. (E) Ratio of Alexa 568 anti-GFP versus L1–GFP signal on the growth cone area, for the different time points and constructs. Data are expressed as mean ± SEM, with (n) the number of growth cones examined, and data were compared by analysis of variance (ANOVA) and Tukey's test (*$p = 0.06$; **$p < 0.01$).

cumulated at L1–Fc-coated microspheres, indicating a preservation of homophilic binding despite the presence of a GFP-tag at the N terminus. This was somewhat expected, because L1–L1 adhesion seems to involve immunoglobulin domains relatively deep in the molecule, in particular Ig2 (Zhao *et al*., 1998) and Ig6 (Itoh *et al*., 2004). Furthermore, L1–L1 binding requires the folding of a hinge region between Ig2 and Ig3 domains (De Angelis *et al*., 2002) and the adoption of a horseshoe conformation (Schurmann *et al*., 2001), in which the N-terminal GFP should not be a hindrance.

Table 2. Turnover rates calculated from FRAP experiments for the various ligand–receptor interactions at bead contacts

	Transfection			
	L1–GFP	L1–GFP	L1–GFPΔCter	NrCAM–GFP
Ligand	L1–Fc	Anti-L1	L1–Fc	TAG-1
k_{off} (h^{-1})	6.1 ± 1.6	1.0 ± 0.5**	2.2 ± 0.8*	0.18 ± 0.07****
n	24	13	17	8

Data are expressed as mean ± SEM, where n is the number of beads tested. Turnover rates were found to be statistically different by ANOVA and compared with the L1–GFP/L1–Fc condition by Tukey's test (*$p = 0.06$; **$p < 0.01$; ****$p < 0.001$). Data for NrCAM-GFP at TAG-1 bead contacts in B104 neuroblastoma cells were obtained previously (Falk *et al*., 2004) and are reanalyzed here.

Exocytosis of L1 Molecules Contribute to the Initiation of L1 Homophilic Adhesions

Using these tools, we detailed the respective contributions of diffusion/trapping versus membrane trafficking in the formation and renewal of L1 adhesions (Figure 9). It was previously shown in DRG neurons that polarized trafficking of L1 molecules through endosomal compartments within the growth cone, allows growth cone migration on an L1 substrate (Kamiguchi and Lemmon, 2000; Kamiguchi and Yoshihara, 2001). However, how exo/endocytosis events were linked to the formation and dissociation of L1 adhesions at the plasma membrane remained unclear. Our experiments with L1–Fc or anti-L1–coated microsphere bring an answer to this question. When L1–Fc-coated microspheres were initially presented to the growth cone, we measured a very rapid increase in L1–GFP receptor accumulation, reaching equilibrium in ~2 min. We calculated that half of the accumulated receptors came from passive

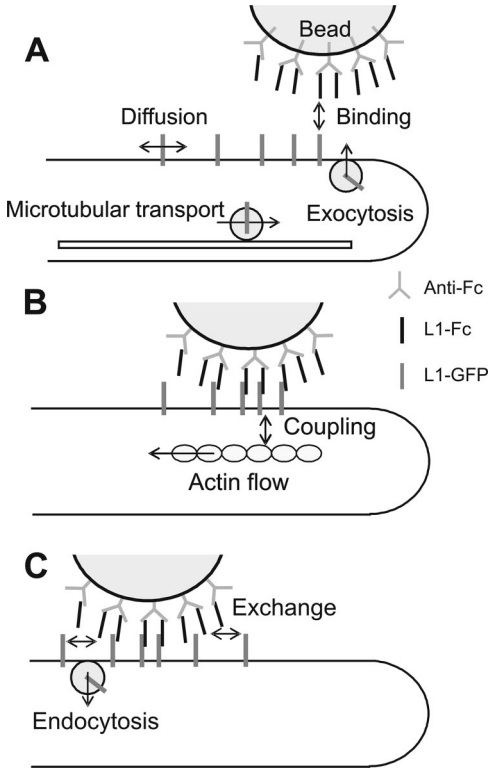

Figure 9. Model showing the cooperation between lateral diffusion and exo/endocytosis events in the dynamics of L1 homophilic contacts. (A) Initial contact formation at the growth cone periphery involves both directed exocytosis and lateral diffusion. (B) Beads rapidly couple to the actin flow and travel to the base of growth cones, as more receptors are being recruited. (C) Mature contacts in the central domain are still capable of turnover and recycle by diffusion/untrapping as well as endocytosis, which occurs preferentially in this region.

membrane diffusion, which we directly visualized in some experiments by the selective trapping of QD-labeled L1–GFP molecules at L1–Fc bead contacts (data not shown). The other half came from freshly exocytosed L1 molecules, likely via the selective transport and delivery of L1–GFP-rich vesicles at the growth cone periphery (Figure 9A). This process was selective of the L1–Fc ligand, because beads coated with anti-L1 (this study) or anti-GFP (Thoumine *et al*., 2005) recruited essentially surface receptors, with a slower rate. Thus, there must be a signaling process specific of the L1–Fc ligand. Accordingly, in DRG neurons the selective addressing of L1 at the growth cone extremity is specific of cells migrating on an L1 substrate, and it does not occur on an N-cadherin substrate (Kamiguchi and Yoshihara, 2001). Overall, L1 molecules accumulate at L1–Fc contacts threefold faster than N-cadherin receptors at Ncad–Fc contacts (Thoumine *et al*., 2006), revealing both a faster homophilic interaction kinetics, and a selective addressing by exocytosis. How is this achieved? It is possible that L1 ligation initiates a signaling pathway that triggers exocytosis of L1-rich vesicles to the nascent contact (for a review of L1 and NCAM-based signaling pathways, see Maness and Schachner, 2007). For example, calcium transients were found to activate VAMP-2–mediated exocytosis involved in growth cone turning on L1–Fc-coated substrates (Tojima *et al*., 2007). We recently reported a close association between L1 adhesions, the SNARE protein TI-VAMP and the actin cytoskeleton in growth cones (Alberts *et al*., 2006). In particular, we showed that TI-VAMP silencing reduces L1 adhesiveness without affecting L1 cell surface expression (Alberts *et al*., 2003). Thus, TI-VAMP could mediate the selective delivery of L1-rich vesicles to the plasma membrane, through a specific association with the actin cytoskeleton recruited at initial L1 contacts. However, this cannot be directly tested in neurons because silencing TI-VAMP's expression also impairs neuritogenesis (Alberts *et al*., 2003).

Ligand-bound or Clustered L1 Molecules Connect to the Actin Flow

A close association of ligand-bound L1 molecules and the actin cytoskeleton was observed, because L1-coated microspheres rapidly coupled to the actin retrograde flow (Figure 9B). Beads slowed down as more L1 molecules accumulated, and they finally stalled when recruitment reached a steady state. In this process, the L1–L1 contact had changed compartments from the peripheral actin-rich lamellipodium to the microtubule rich central region of the growth cone. The bead velocity was the exact mirror image of L1–GFP receptor recruitment, suggesting that the connection to the actin flow could control the rate of L1–GFP receptor accumulation. This strong interaction may involve actin binding partners such as ERM or ankyrin. Indeed, L1 molecules bound to L1–Fc were shown to couple to the actin flow via ankyrin B in the neuronal perisomatic lamellae (but not in growth cones), promoting neurite initiation (Nishimura *et al*., 2003). In contrast, a study using L1 molecules mutated in the cytoplasmic domain and expressed in L1 knockout neuronal cultures showed instead that the L1–ERM but not the L1–ankyrin interactions were essential for neurite outgrowth (Cheng *et al*., 2005).

It was intriguing that individual L1–GFP molecules labeled with quantum dots moved randomly on the surface of growth cones, with no apparent retrograde component. One explanation can be that cell adhesion molecules require a certain degree of clustering to engage in various functions, e.g., trimers of L1 are more potent than monomers in terms of adhesiveness and promotion of neurite outgrowth (Hall *et al*., 2000), whereas integrin trimerization is required for the anchoring to actin (Coussen *et al*., 2002). Due to their small size (i.e., roughly 25 nm in diameter), QDs are presumably attached to one or very few L1 molecules, apparently not enough to trigger their connection to the actin flow. Indeed, beads of intermediate size coated with anti-L1 or L1–Fc ligands show a complex behavior, with a fraction of them moving rearward, some diffusing, and others staying associated with static components of the cytoskeleton (Kamiguchi and Yoshihara, 2001; Gil *et al*., 2003; Falk *et al*., 2004). Ligand activation of L1 molecules may be necessary to further engage L1 into cytoskeletal binding (Nishimura *et al*., 2003), and this was not achieved using single molecule detection with a nonperturbing anti-GFP antibody.

The immobilization of individual L1 molecules may also involve several interacting proteins. L1 can bind ankyrin, this interaction being promoted by the dephosphorylation of the tyrosine in a FIGQY motif situated in the L1 intracellular region (Garver *et al*., 1997; Tuvia *et al*., 1997) and regulated through the mitogen-activated protein kinase pathway (Whittard *et al*., 2006). Growth cones are enriched in ankyrin B (Nishimura *et al*., 2003) and poorly stained by an antibody against phosphorylated FIGQY, suggesting that L1 is mainly in a dephosphorylated form thus available for ankyrin binding (Boiko *et al*., 2007). Indeed, ankyrin was shown to mediate the coupling of L1 with a static actin network in neuroblastoma cells (Gil *et al*., 2003). Therefore, the increase in mobility observed here for the L1ΔCter mutant can be partly explained by a lack of interaction with ankyrin B. The relatively mild phenotype may be due to the formation of *cis*-dimers between L1ΔCter and endogenous L1, e.g., involving the third FnIII domain (Silletti *et al*., 2000). However, using NrCAM molecules in which the FnIII domains were replaced by GFP, we also observed a very small increase in NrCAM lateral mobility upon truncation of the C-tail upstream of the ankyrin binding sequence (Thoumine *et al*., 2005). Together, these findings indicate that ankyrin is a mild regulator of L1 stabilization in our experimental model. Interactions of L1 with ERM or the clathrin adaptor AP-2 might be more important.

Contribution of Endocytosis in the Fast Turnover of Mature L1 Adhesions

Although reaching equilibrium, L1–L1 adhesions stayed highly dynamic as revealed by FRAP experiments (Figure 9C). The turnover of L1 homophilic adhesions was twice as large as that measured previously for N-cadherin adhesions (Thoumine *et al*., 2006), and it was 30-fold higher than the adhesions formed between TAG-1 and NrCAM (Falk *et al*., 2004). Such fast renewal of L1–L1 bonds implicated an exchange with unbleached L1–GFP molecules that could come either by diffusion at the plasma membrane or from trafficking events. Exocytosis was not involved in this latter case, because no recovery of L1–GFP fluorescence was observed around stable L1–Fc bead contacts after thrombin treatment. Thus, exocytosis is specific of the initial phase of L1–L1 bond formation at the growth cone periphery, and no longer acts in more mature adhesions in the central region. In contrast, the central domain is a region of preferential endocytosis, as revealed by antibody feeding assay and in agreement with previous studies using DRG neurons (Kamiguchi and Lemmon, 2000; Kamiguchi and Yoshihara, 2001). Such internalization of L1 molecules may be due to a specific interaction of L1 with endocytotic clathrin-coated pits, e.g., through the AP-2 complex that can interact specifically with an YRSLE sequence located on the neuronal L1 cytoplasmic tail (Kamiguchi *et al*., 1998b; Kamiguchi and Yoshihara,

2001). This suggested a role of endocytosis in the renewal of L1 adhesions at the base of growth cones.

Indeed, the truncated receptor L1–GFPΔCter showed a significantly reduced turnover rate in FRAP experiments at stable L1–Fc bead contacts. It was previously shown that L1 molecules deleted of the RSLE internalization sequence increase cell aggregation compared with wild-type counterparts, while keeping a similar surface expression (Long *et al*., 2001). This surprising effect was proposed to be due to fast attachment/detachment kinetics of L1–L1 adhesions, making free wild-type receptors readily endocytosed. Here, we directly demonstrate that L1–L1 homophilic bonds are indeed very labile and that L1–GFPΔCter molecules that are less endocytosed have a smaller turnover rate, contributing to more stable L1 adhesions. An increase in L1–L1 affinity for the L1–ΔCter mutant, similar to that reported recently for N-cadherin (Thoumine *et al*., 2006), is unlikely, because the L1 cytoplasmic tail is dispensable for homophilic adhesion (Wong *et al*., 1995). Immobilization and endocytosis of L1–ΔCter molecules were not totally prevented, possibly because of a clathrin-independent endocytotic pathway, or the role of lateral association of mutated receptors with endogenous receptors in the plasma membrane, e.g., L1 itself, other IgCAMs, or integrins (Silletti *et al*., 2000; Brummendorf and Lemmon, 2001; Cheng *et al*., 2005). Indeed, the replacement of the FnIII domains by GFP in the homologue molecule NrCAM (Falk *et al*., 2004), thus preventing *cis*-oligomerization (Silletti *et al*., 2000), was accompanied by an important decrease in endocytosis rate. It is not clear what triggers the transition between L1 coupling to the actin flow and L1 endocytosis, but it may involve the coordinated phosphorylation and dephosphorylation events of critical tyrosine residues in the L1 cytoplasmic tail. Indeed, phosphorylation of Y1229 induces uncoupling of neurofascin and L1 from ankyrin (Garver *et al*., 1997; Needham *et al*., 2001; Gil *et al*., 2003), whereas dephosphorylation of Y1176 after L1 liganding or cross-linking allows binding to AP-2 (Schaefer *et al*., 2002). A switch from ezrin to AP-2 binding, which compete for the same site on the juxtamembrane domain of L1 (Cheng *et al*., 2005), is also possible.

CONCLUSIONS

Our data reveal in fine detail the physical mechanisms governing the dynamics of L1 adhesions underlying growth cone motility. They highlight the coordination between the processes of exo/endocytosis of L1 molecules, the role of membrane diffusion, and the kinetics of L1–L1 bonds, which altogether result in a rapid turnover of L1 contacts. The L1 molecule is unique in this respect, because NrCAM or N-cadherin, which are less internalized, both make much more stable adhesions (Falk *et al*., 2004; Thoumine *et al*., 2006). This fast renewal of L1 molecules may be essential to processes of axon elongation and fasciculation requiring reactive adhesiveness at the growth cone.

ACKNOWLEDGMENTS

We thank Y. Goldberg for the transfection protocol; P. Gonzales for coverslip preparation, D. Bouchet, C. Breillat, and B. Tessier for neuronal cultures and DNA preparations; L. Cognet and M. Renner for QD tracking algorithms; M. Heine for the QD coupling protocol; D. Perrais and S. Lacroix-Desmazes for thrombin inhibitors; and J. Falk, M. Lambert, R. M. Mège, E. Petrini, and C. Sarrailh for critical reading of the manuscript. We acknowledge financial support from Centre National de la Recherche Scientifique and Conseil Régional Aquitaine (to C.D., O.T., and D.C.) and from Institut National de la Santé et de la Recherche Médicale (Avenir Program), European Commission ("Signaling and Traffic" STREP 503229), Association Française contre les Myopathies, French Ministry of Research (ACI-BDP), Fondation pour la Recherche Médicale, and Fondation pour la Recherche sur le Cerveau (to T.G.). L.D. was supported by a postdoctoral fellowship from the Association pour la Recherche sur le Cancer.

REFERENCES

Alberts, P. *et al*. (2003). Cross talk between tetanus neurotoxin-insensitive vesicle-associated membrane protein-mediated transport and L1-mediated adhesion. Mol. Biol. Cell *14*, 4207–4220.

Alberts, P., Rudge, R., Irinopoulou, T., Danglot, L., Gauthier-Rouviere, C., and Galli, T. (2006). Cdc42 and actin control polarized expression of TI-VAMP vesicles to neuronal growth cones and their fusion with the plasma membrane. Mol. Biol. Cell *17*, 1194–1203.

Boiko, T., Vakulenko, M., Ewers, H., Yap, C. C., Norden, C., and Winckler, B. (2007). Ankyrin-dependent and -independent mechanisms orchestrate axonal compartmentalization of L1 family members neurofascin and L1/neuron-glia cell adhesion molecule. J. Neurosci. *27*, 590–603.

Brewer, G. J. (1996). Thrombin causes cell spreading and redistribution of beta-amyloid immunoreactivity in cultured hippocampal neurons. J. Neurochem. *67*, 119–130.

Brummendorf, T., and Lemmon, V. (2001). Immunoglobulin superfamily receptors: cis-interactions, intracellular adapters and alternative splicing regulate adhesion. Curr. Opin. Cell Biol. *13*, 611–618.

Cheng, L., Itoh, K., and Lemmon, V. (2005). L1-mediated branching is regulated by two ezrin-radixin-moesin (ERM)-binding sites, the RSLE region and a novel juxtamembrane ERM-binding region. J. Neurosci. *25*, 395–403.

Coussen, F., Choquet, D., Sheetz, M. P., and Erickson, H. P. (2002). Trimers of the fibronectin cell adhesion domain localize to actin filament bundles and undergo rearward translocation. J. Cell Sci. *115*, 2581–2590.

Davey, F., Hill, M., Falk, J., Sans, N., and Gunn-Moore, F. J. (2005). Synapse associated protein 102 is a novel binding partner to the cytoplasmic terminus of neurone-glial related cell adhesion molecule. J. Neurochem. *94*, 1243–1253.

De Angelis, E., MacFarlane, J., Du, J. S., Yeo, G., Hicks, R., Rathjen, F. G., Kenwrick, S., and Brummendorf, T. (1999). Pathological missense mutations of neural cell adhesion molecule L1 affect homophilic and heterophilic binding activities. EMBO J *18*, 4744–4753.

De Angelis, E., Watkins, A., Schafer, M., Brummendorf, T., and Kenwrick, S. (2002). Disease-associated mutations in L1 CAM interfere with ligand interactions and cell-surface expression. Hum. Mol. Genet. *11*, 1–12.

Dent, E. W., and Gertler, F. B. (2003). Cytoskeletal dynamics and transport in growth cone motility and axon guidance. Neuron *40*, 209–227.

Dickson, T. C., Mintz, C. D., Benson, D. L., and Salton, S. R. (2002). Functional binding interaction identified between the axonal CAM L1 and members of the ERM family. J. Cell Biol. *157*, 1105–1112.

Diefenbach, T. J., Latham, V. M., Yimlamai, D., Liu, C. A., Herman, I. M., and Jay, D. G. (2002). Myosin 1c and myosin IIB serve opposing roles in lamellipodial dynamics of the neuronal growth cone. J. Cell Biol. *158*, 1207–1217.

Donovan, F. M., Pike, C. J., Cotman, C. W., and Cunningham, D. D. (1997). Thrombin induces apoptosis in cultured neurons and astrocytes via a pathway requiring tyrosine kinase and RhoA activities. J. Neurosci. *17*, 5316–5326.

Falk, J., Thoumine, O., Dequidt, C., Choquet, D., and Faivre-Sarrailh, C. (2004). NrCAM coupling to the cytoskeleton depends on multiple protein domains and partitioning into lipid rafts. Mol. Biol. Cell *15*, 4695–4709.

Garver, T. D., Ren, Q., Tuvia, S., and Bennett, V. (1997). Tyrosine phosphorylation at a site highly conserved in the L1 family of cell adhesion molecules abolishes ankyrin binding and increases lateral mobility of neurofascin. J. Cell Biol. *137*, 703–714.

Gil, O. D., Sakurai, T., Bradley, A. E., Fink, M. Y., Cassella, M. R., Kuo, J. A., and Felsenfeld, D. P. (2003). Ankyrin binding mediates L1CAM interactions with static components of the cytoskeleton and inhibits retrograde movement of L1CAM on the cell surface. J. Cell Biol. *162*, 719–730.

Goslin, K., Asmussen, H., and Banker, G. (1991). Rat hippocampal neurons in low-density culture. In: Culturing Nerve Cells, ed. G. Banker and K. Goslin, Cambridge, MA: The MIT Press, 339–370.

Hall, H., Bozic, D., Fauser, C., and Engel, J. (2000). Trimerization of cell adhesion molecule L1 mimics clustered L1 expression on the cell surface: influence on L1-ligand interactions and on promotion of neurite outgrowth. J. Neurochem. *75*, 336–346.

Horinouchi, K., Nakamura, Y., Yamanaka, H., Watabe, T., and Shiosaka, S. (2005). Distribution of L1cam mRNA in the adult mouse brain: in situ hybridization and Northern blot analyses. J. Comp. Neurol. *482*, 386–404.

Itoh, K., Cheng, L., Kamei, Y., Fushiki, S., Kamiguchi, H., Gutwein, P., Stoeck, A., Arnold, B., Altevogt, P., and Lemmon, V. (2004). Brain development in mice lacking L1–L1 homophilic adhesion. J. Cell Biol. *165*, 145–154.

Itoh, K., Shimono, K., and Lemmon, V. (2005). Dephosphorylation and internalization of cell adhesion molecule L1 induced by theta burst stimulation in rat hippocampus. Mol. Cell Neurosci. *29*, 245–249.

Kamiguchi, H., Hlavin, M. L., and Lemmon, V. (1998a). Role of L1 in neural development: what the knockouts tell us. Mol. Cell Neurosci. *12*, 48–55.

Kamiguchi, H., and Lemmon, V. (2000). Recycling of the cell adhesion molecule L1 in axonal growth cones. J. Neurosci. *20*, 3676–3686.

Kamiguchi, H., Long, K. E., Pendergast, M., Schaefer, A. W., Rapoport, I., Kirchhausen, T., and Lemmon, V. (1998b). The neural cell adhesion molecule L1 interacts with the AP-2 adaptor and is endocytosed via the clathrin-mediated pathway. J. Neurosci. *18*, 5311–5321.

Kamiguchi, H., and Yoshihara, F. (2001). The role of endocytic l1 trafficking in polarized adhesion and migration of nerve growth cones. J. Neurosci. *21*, 9194–9203.

Koroll, M., Rathjen, F. G., and Volkmer, H. (2001). The neural cell recognition molecule neurofascin interacts with syntenin-1 but not with syntenin-2, both of which reveal self-associating activity. J. Biol. Chem. *276*, 10646–10654.

Long, K. E., Asou, H., Snider, M. D., and Lemmon, V. (2001). The role of endocytosis in regulating L1-mediated adhesion. J. Biol. Chem. *276*, 1285–1290.

Maness, P. F., and Schachner, M. (2007). Neural recognition molecules of the immunoglobulin superfamily: signaling transducers of axon guidance and neuronal migration. Nat. Neurosci. *10*, 19–26.

Miller, P. D., Chung, W. W., Lagenaur, C. F., and DeKosky, S. T. (1993). Regional distribution of neural cell adhesion molecule (N-CAM) and L1 in human and rodent hippocampus. J. Comp. Neurol. *327*, 341–349.

Munakata, H., Nakamura, Y., Matsumoto-Miyai, K., Itoh, K., Yamasaki, H., and Shiosaka, S. (2003). Distribution and densitometry mapping of L1-CAM immunoreactivity in the adult mouse brain–light microscopic observation. BMC Neurosci. *4*, 7.

Needham, L. K., Thelen, K., and Maness, P. F. (2001). Cytoplasmic domain mutations of the L1 cell adhesion molecule reduce L1-ankyrin interactions. J. Neurosci. *21*, 1490–1500.

Nishimura, K., Yoshihara, F., Tojima, T., Ooashi, N., Yoon, W., Mikoshiba, K., Bennett, V., and Kamiguchi, H. (2003). L1-dependent neuritogenesis involves ankyrinB that mediates L1-CAM coupling with retrograde actin flow. J. Cell Biol. *163*, 1077–1088.

Pollerberg, G. E., Nolte, C., and Schachner, M. (1990). Accumulation of N-CAM 180 at contact sites between neuroblastoma cells and latex beads coated with extracellular matrix molecules. Eur. J. Neurosci. *2*, 879–887.

Racine, V., Hertzog, A., Jouanneau, J., Salamero, J., Kervrann, C., and Sibarita, J. (2006). Multiple target tracking of 3D fluorescent objects based on simulated annealing. In: Biomedical Imaging: Nano to Macro, 2006. 3rd IEEE International Symposium on Biomedical Imaging, 1020–1023. April 6–9, 2006, Arlington, VA.

Sampo, B., Kaech, S., Kunz, S., and Banker, G. (2003). Two distinct mechanisms target membrane proteins to the axonal surface. Neuron *37*, 611–624.

Sasakura, H., Inada, H., Kuhara, A., Fusaoka, E., Takemoto, D., Takeuchi, K., and Mori, I. (2005). Maintenance of neuronal positions in organized ganglia by SAX-7, a *Caenorhabditis elegans* homologue of L1. EMBO J. *24*, 1477–1488.

Schaefer, A. W., Kamei, Y., Kamiguchi, H., Wong, E. V., Rapoport, I., Kirchhausen, T., Beach, C. M., Landreth, G., Lemmon, S. K., and Lemmon, V. (2002). L1 endocytosis is controlled by a phosphorylation-dephosphorylation cycle stimulated by outside-in signaling by L1. J. Cell Biol. *157*, 1223–1232.

Schurmann, G., Haspel, J., Grumet, M., and Erickson, H. P. (2001). Cell adhesion molecule L1 in folded (horseshoe) and extended conformations. Mol. Biol. Cell *12*, 1765–1773.

Sheetz, M. P., Baumrind, N. L., Wayne, D. B., and Pearlman, A. L. (1990). Concentration of membrane antigens by forward transport and trapping in neuronal growth cones. Cell *61*, 231–241.

Silletti, S., Mei, F., Sheppard, D., and Montgomery, A. M. (2000). Plasmin-sensitive dibasic sequences in the third fibronectin-like domain of L1-cell adhesion molecule (CAM) facilitate homomultimerization and concomitant integrin recruitment. J. Cell Biol. *149*, 1485–1502.

Suter, D. M., Errante, L. D., Belotserkovsky, V., and Forscher, P. (1998). The Ig superfamily cell adhesion molecule, apCAM, mediates growth cone steering by substrate-cytoskeletal coupling. J. Cell Biol. *141*, 227–240.

Tardin, C., Cognet, L., Bats, C., Lounis, B., and Choquet, D. (2003). Direct imaging of lateral movements of AMPA receptors inside synapses. EMBO J. *22*, 4656–4665.

Thoumine, O., Lambert, M., Mege, R. M., and Choquet, D. (2006). Regulation of N-cadherin dynamics at neuronal contacts by ligand binding and cytoskeletal coupling. Mol. Biol. Cell *17*, 862–875.

Thoumine, O., Saint-Michel, E., Dequidt, C., Falk, J., Rudge, R., Galli, T., Faivre-Sarrailh, C., and Choquet, D. (2005). Weak effect of membrane diffusion on the rate of receptor accumulation at adhesive contacts. Biophys. J. *89*, L40–42.

Tojima, T., Akiyama, H., Itofusa, R., Li, Y., Katayama, H., Miyawaki, A., and Kamiguchi, H. (2007). Attractive axon guidance involves asymmetric membrane transport and exocytosis in the growth cone. Nat. Neurosci. *10*, 58–66.

Tuvia, S., Garver, T. D., and Bennett, V. (1997). The phosphorylation state of the FIGQY tyrosine of neurofascin determines ankyrin-binding activity and patterns of cell segregation. Proc. Natl. Acad. Sci. USA *94*, 12957–12962.

Whittard, J. D., Sakurai, T., Cassella, M. R., Gazdoiu, M., and Felsenfeld, D. P. (2006). MAP kinase pathway-dependent phosphorylation of the L1-CAM ankyrin binding site regulates neuronal growth. Mol. Biol. Cell *17*, 2696–2706.

Wisco, D., Anderson, E. D., Chang, M. C., Norden, C., Boiko, T., Folsch, H., and Winckler, B. (2003). Uncovering multiple axonal targeting pathways in hippocampal neurons. J. Cell Biol. *162*, 1317–1328.

Wong, E. V., Cheng, G., Payne, H. R., and Lemmon, V. (1995). The cytoplasmic domain of the cell adhesion molecule L1 is not required for homophilic adhesion. Neurosci. Lett. *200*, 155–158.

Xia, Z., Dudek, H., Miranti, C. K., and Greenberg, M. E. (1996). Calcium influx via the NMDA receptor induces immediate early gene transcription by a MAP kinase/ERK-dependent mechanism. J. Neurosci. *16*, 5425–5436.

Yang, Y., Akiyama, H., Fenton, J. W., 2nd, and Brewer, G. J. (1997). Thrombin receptor on rat primary hippocampal neurons: coupled calcium and cAMP responses. Brain Res. *761*, 11–18.

Zhao, X., Yip, P. M., and Siu, C. H. (1998). Identification of a homophilic binding site in immunoglobulin-like domain 2 of the cell adhesion molecule L1. J. Neurochem. *71*, 960–971.